



ORIGINAL ARTICLE

In-silico screening based on molecular simulations of 3,4-disubstituted pyrrolidine sulfonamides as selective and competitive GlyT1 inhibitors



Mohamed El fadili ^{a,*}, Mohammed Er-rajj ^a, Wafa Ali Eltayb ^b, Mohammed Kara ^{c,**}, Amine Assouguem ^d, Asmaa Saleh ^e, Omkulthom Al Kamaly ^e, Sara Zarougui ^a, Menana Elhallaoui ^a

^a LIMAS Laboratory, Faculty of Sciences Dhar El Mehraz, Sidi Mohammed Ben Abdellah University, BP 1796 Atlas, Fez 30000, Morocco

^b Biotechnology Department, Faculty of Sciences and Technology, Shendi University, Shendi 11111, Sudan

^c Laboratory of Biotechnology, Conservation and Valorization of Natural Resources, Faculty of Sciences Dhar El Mehraz, Sidi Mohamed Ben Abdellah University, BP 1796 Atlas, Fez, Morocco

^d Laboratory of Functional Ecology and Environment, Faculty of Sciences and Technology, Sidi Mohamed Ben Abdellah University, Imouzzet Street, Fez P.O. Box 2202, Morocco

^e Department of Pharmaceutical Sciences, College of Pharmacy, Princess Nourah bint Abdulrahman University, P.O. Box 84428, Riyadh 11671, Saudi Arabia

Received 8 February 2023; accepted 21 June 2023

Available online 28 June 2023

KEYWORDS

NMDA;
GlyT1;
ADME-Toxicity;
CNS;
MD

Abstract A systematic in-silico study based on molecular modeling techniques was conducted on thirty 3,4-disubstituted pyrrolidine sulfonamides derivatives to identify the drug candidate for treating schizophrenia and impairments associated with NMDA receptor hypofunction, through selective and competitive inhibition of GlyT1. QSAR analysis demonstrates that geometric and constitutional descriptors have a key function in human GlyT1 activity. The in-silico study concluded that the most active ligand labeled C19 was predicted to be a non-toxic inhibitor, with a desired ADME-Toxicity profile and a significant probability to penetrate the central nervous system (CNS). Molecular docking simulations confirmed that the C19 compound was docked to the active sites of drosophila melanogaster dopamine transporter (DAT) protein, creating a variety of chem-

** Corresponding author.

* Corresponding author.

E-mail addresses: Mohamed.elfadili@usmba.ac.ma (M. El fadili), Mohammed.kara@usmba.ac.ma (M. Kara).

Peer review under responsibility of King Saud University.



ical bonds towards TYR 124, ASP 475, GLU 480, ALA 479, and VAL 120 amino acids residues. The molecular dynamic (MD) technique combined with the MMGBSA approach confirmed that produced intermolecular interactions for the (DAT protein–C19 ligand) complex remain so stable during 100 ns of MD simulation time. Consequently, the C19 ligand is highly recommended for the treatment of schizophrenia and other disabilities linked to the hypofunction of glutaminergic NMDA receptors.

© 2023 The Author(s). Published by Elsevier B.V. on behalf of King Saud University. This is an open access article under the CC BY-NC-ND license (<http://creativecommons.org/licenses/by-nc-nd/4.0/>).

1. Introduction

Over the last decade, the glycine transporter type 1 (GlyT1) localized at glutamatergic synapses has gained great attention as one of the major neurotransmitters that control memory and learning functions, and a key element of glycine metabolism in the central nervous system (CNS) (Eulenburg et al., 2005; Hudson et al., 2020; Lowe et al., 2009; Santora et al., 2018). Many pharmaceutical companies have focused on developing selective and competitive GluT1 inhibitors, to provide potential treatments for neurodegenerative disorders associated with glutamine N-methyl-D-aspartate (NMDA) receptor hypofunction, including schizophrenia (Atkinson et al., 2001; Ouellet et al., 2011; Wolkenberg and Sur, 2010; Wolkenberg et al., 2009). A number of these GlyT1 inhibitors have been repeatedly proven to be effective and successful in animal models of schizophrenia and clinically assessed for several symptom domains (Blackaby et al., 2010; Pinard et al., 2010a; Santora et al., 2018). A few years ago, Roche succeeded in developing a noncompetitive GlyT1 inhibitor as the most advanced compound, namely bitopertin (RG1678), which attained positive results to treat negative symptoms of schizophrenia patients. However, it did not successfully reduce these negative symptoms in the later stages of clinical trials, due to its very limited efficacy (Alberati et al., 2012; Pinard et al., 2010a). For this reason, the discovery of selective and competitive glycine transporter type 1 inhibitors continues to be of great interest to chemists in a wide range of literature (Amberg et al., 2018; Blackaby et al., 2010; Hudson et al., 2020; Łatka and Bajda, 2022; Pinard et al., 2010b; Rosenbrock et al., 2023; Santora et al., 2018). Recently, a structural family of 3,4-disubstituted pyrrolidine sulfonamides, was synthesized and experimentally evaluated through in vivo and in vitro assays to selectively and competitively inhibit the glycine transporter type 1. In this regard, our in-silico investigations were carried out on thirty derivatives of 3,4-disubstituted pyrrolidine sulfonamides which were detected thanks to their inhibitory activity against the type 1 of glycine transporter (Wang et al., 2018). In the beginning, we applied the quantitative structure–activity relationship (QSAR), which gained an advanced position in modern chemistry (Vilar et al., 2008), by developing two validated QSAR models which will be able to predict human GluT1 activity for 3,4-disubstituted pyrrolidine sulfonamides family, using multiple linear regression (MLR) and multiple nonlinear regression (MNL) techniques (Mostoufi and Constantinides, 2023). Thereafter, we predicted the physicochemical and pharmacokinetic properties of candidate inhibitors able to cross the blood–brain barrier (BBB), penetrating the central nervous system (CNS). Afterwards, the most active inhibitor having an excellent absorption, distribution, metabolism, excretion, and toxicity (ADME-Tox) profile and meeting all drug-likeness conditions (Tian et al., 2015), was chosen for molecular docking simulation as a technology widely applied in the field of drug discovery (Serrano et al., 2020), indicating the intermolecular interactions produced towards the dopamine transporter membrane protein encoded as 4 M48.pdb <https://www.rcsb.org/structure/4M48> (Bank, n.d.). Moreover, the process of molecular docking for the (candidate ligand-targeted protein) complex was successfully validated using the docking validation protocol (El fadili et al., 2022a). The molecular stability of the studied complex was examined with the help of the molecular dynamics (MD) technique during 100 ns of MD simulation time,

studying the conformational changes behaviors of the targeted protein towards the candidate drug with detailed temporal resolution and highest atomic precision (El fadili et al., 2022b; Hollingsworth and Dror, 2018; Hu et al., 2023; Karplus and McCammon, 2002). Finally, the molecular mechanics with generalized born and surface area (MMGBSA) solvation was equally conducted to calculate the binding free energies of the studied complex, to check again the molecular stability of the candidate ligand in complex with the protein target (Faisal et al., 2022; Ononamadu et al., 2021). Thus, the present study aims to discover a highly effective drug among thirty selective and competitive GluT1 inhibitors, predicted with a good ADME-Toxicity profile, and defined with a good level of molecular stability towards the targeted protein, which we can strongly recommend for the treatment of schizophrenia and other impairments associated with NMDA receptor hypofunction.

2. Materials and methods

2.1. Experimental database

The present work aims to study thirty of 3,4-disubstituted pyrrolidine sulfonamides shown in Table S1 (Wang et al., 2018), whose the human GlyT1 activities of Ki order were converted to pKi scale ($pK_i = -\log_{10} K_i$), and the experimental database was divided on training and test sets which contain 80 % and 20 % of active molecules, respectively.

2.2. Molecular descriptors calculation

To develop the quantitative structure–activity relationships (QSAR), a number of molecular descriptors were calculated, as resulted in Table S2. The constitutional descriptors were executed using ACD/chemsketch software (Österberg and Norinder, 2001), while the geometric, physicochemical, thermodynamic, and topological descriptors were obtained using ChemBio3D software (Milne, 2010).

2.3. Statistical methods

Initially, the principal component analysis (PCA) was applied as a multivariate statistical method, to reduce the dimension of calculated descriptors based on the correlation matrix, in which the non-correlated descriptors were kept well, while one of the two highly correlated descriptors (r greater than 0.9) was removed (Groth et al., 2013; Guerra Tort et al., 2020; Maćkiewicz and Ratajczak, 1993). Secondly, the linear and nonlinear relationships between human GluT1 activity and uncorrelated descriptors were studied using multiple linear regression (MLR) and multiple nonlinear regression (MNL) techniques, respectively (Mostoufi and Constantinides, 2023). So, MLR and MNL QSAR models, which were developed

for training set of 24 molecules, were externally validated for test set on 6 novel molecules. Moreover, the mathematical models were internally validated with the help of cross validation with the leave one out procedure (CV-LOO) (Er-Rajy et al., 2022).

2.4. In-silico pharmacokinetics, drug-likeness, and ADMET depiction exploration

Before proceeding with any clinical investigation, it is necessary to carry out an assessment of absorption, distribution, metabolism, excretion and toxicity (ADME-Tox) properties in the human body, checking the five rules of Lipinski (Lipinski et al., 1997), and respecting the violations number of Veber, Ghose, Egan, and Muegge (Egan et al., 2000; Egan and Lauri, 2002; Muegge et al., 2001; Veber et al., 2002) for the drug candidates, which were predicted as central nervous system (CNS) agents according to Boild-Eggs model. To achieve this objective, we examined the physicochemical and in-silico pharmacokinetics properties of the candidate's compounds, with the help of pkCSM (Pires et al., 2015), and SwissADME ("SwissADME," n.d.) servers.

2.5. Molecular docking simulation

To discover the chemical bonds produced between a drug candidate and a target protein, we performed molecular docking, an effective drug discovery technique (Bassani et al., 2022). The dopamine transport protein, was uploaded from proteins data bank (PDB), which was discovered by the X-ray diffraction technique with a resolution of 2.96 Å (Bank, n.d.; Kouranov, 2006). The targeted protein coded as 4 M48.pdb was prepared using Discovery Studio 2021 (BIOVIA) software package (Systèmes, 2020), removing the water molecules (H₂O), chloride and sodium ions (Na⁺, Cl⁻) and all suspended ligands like as cholesterol (C₂₇H₄₆O) and nortriptyline (C₁₉H₂₁N). The gasteiger charges and polar hydrogens were added. Then, the prepared protein was docked to the candidate drug using AutoDock 4.2 software (Norgan et al., 2011), converting the complex to PDBQT format. The sizes of grid box were centralized on (-42.424 Å, -0.573 Å, 55.066 Å), putting the 3D- structure dimensions on (120, 120, 120) with a spacing of 0.375 Å. Finally, the results of intermolecular interactions produced for the most stable complex were visualized by mean of Discovery Studio 2021 (BIOVIA) software.

2.6. Molecular dynamic

To investigate the stability of intermolecular interactions produced between the candidate drug and targeted protein, we performed the molecular dynamics for studied complex during 100 ns of simulation time, using Desmond software, a package of Schrödinger LLC (Pyrhönen et al., 2022). The (candidate drug-targeted protein) complex was prepared with the assistance of Protein Preparation Maestro. Then, the pre-treated complex was optimized in the System Builder, working on a solvent model of TIP3P orthorhombic box, with application of OPLS force field (Kaminski et al., 2001). Additionally, the selected model was neutralized by the reproduction of physiological conditions, adding water molecules (H₂O) and counter

ions ([Na⁺, Cl⁻] equal to 0.15 M) with a temperature of 300 K and a pressure of 1 atm.

3. Results and discussion

3.1. Quantitative structure-activity relationships (QSARs)

3.1.1. Principal components analysis

The quantitative structure-activity relationship technique is intended to develop a predictive QSAR model between biological activity and uncorrelated descriptors. For this goal, we applied the principal component analysis (PCA) as a statistical method widely applied to minimize the size of molecular descriptors in a reduced number of factorial axes (or principal components) based on the correlation matrix (Bastianoni et al., 2021), as resulted in Table S2, which indicates thirty-two strong correlations (correlation coefficients of Pearson superior than 0.9). So, the development of QSAR model was focused only on weakly correlated descriptors.

3.1.2. Multiple linear regression

To study the linear relationship between the structural descriptors and human GluT1 activity, we applied the multiple linear regression (MLR) technique (Uyanık and Güler, 2013) on 24 molecules of training set, based on stepwise selection for hundreds of randomizations. Therefore, the best MLR QSAR model was obtained in equation (1), considering the best values of determination, adjustment, and correlation coefficients (R^2 , R^2 adjusted, and R) and minimal root mean square deviation (RMSD).

$$pKi = -60.528 + 43.061 \times D + 3.569 \times \%H + 0.321 \\ \times VDWE - 0.087 \times TE - 0.642 \times \%N - 0.539 \\ \times \%O \quad (1)$$

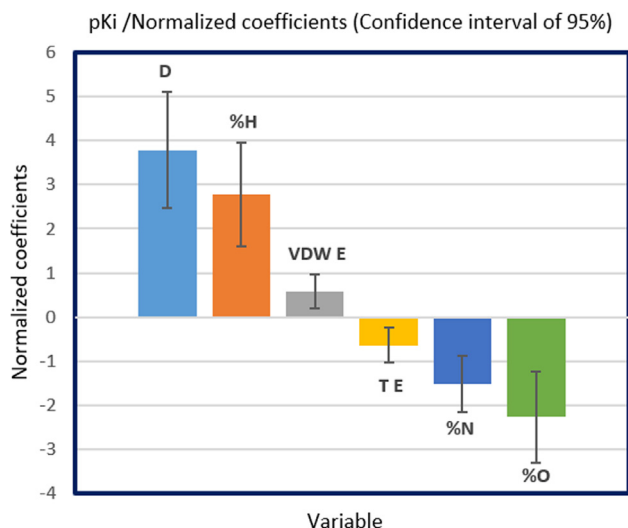
The first predictive QSAR model developed in equation (1), demonstrates that human GluT1 activity of pKi order is strongly correlated with constitutional descriptors (in particular %H, %N, %O and D) and geometric descriptors (like as T E, and VDW E), with minimal root mean square deviation (RMSD of 0.546) and good values of determination, correlation, and adjustment coefficients ($R^2 = 0.746$, R^2 adjusted = 0.657, and $R = 0.864$, respectively). The six selected descriptors (Table S3) have significant impacts on human GluT1 activity, because the slope of each one is defined by a probability < 0.05 (5%) for 95% of confidence interval, as displayed in Table 1.

The developed MLR model shows that electronic density (D), mass percentage of hydrogen (%H), and van der Waals energy (VDW E) have a positive effect on human GluT1 activity, but mass percentages of nitrogen and oxygen (%N, %O), and torsion energy (T E) affect it negatively, as displayed in Fig. 1.

The analysis of variance (Anova test) shows that calculated value of Fisher ($F = 8.332$) is superior to its critical value ($F(30, 6) = 2.42$, $p < 5\%$), which indicates that null hypothesis (H₀) was rejected, so there is an homogenous variance between the inhibitory activity and six selected descriptors as displayed in Table 2.

Table 1 The significant weights of the selected descriptors.

Source	Value	Standard deviation	t	Pr > t	Lower terminal (95%)	Higher terminal (95%)
Constante	-60.528	12.047	-5.024	0.000	-85.945	-35.111
D	43.061	7.133	6.037	< 0.0001	28.011	58.110
%H	3.569	0.710	5.025	0.000	2.071	5.068
VDW E	0.321	0.101	3.162	0.006	0.107	0.534
T E	-0.087	0.026	-3.366	0.004	-0.142	-0.033
%N	-0.642	0.129	-4.969	0.000	-0.915	-0.369
%O	-0.539	0.117	-4.628	0.000	-0.785	-0.293

**Fig. 1** The impact of selected descriptors on human GluT1 activity.

3.2. Multiple non-linear regression

To model the nonlinear regression between the six uncorrelated descriptors, signaled by MLR method and GlyT1 activity, we performed the multiple non-linear regression (MNL) method (Kravić et al., 2022), for twenty-four inhibitors (training set) based on following programmed function:

$$Y = a_0 + \sum_{i=1}^n (a_i \times X_i + b_i \times X_i^2)$$

(El fadili et al., 2022b) Y: predicted activity by MNL QSAR model. a_0 : constant of predictive model. X_i : selected descriptor. a_i , b_i : slopes of each descriptor for one and two degrees, respectively.

The second QSAR model, developed by the pre-programmed function of multiple non-linear regression con-

firms also that human GluT1 activity of pki order is affected by the six selected descriptors as expressed in equation (2). This mathematical model is done by a low deviation (RMSD equal to 0.636) and good values of determination and correlation coefficients ($R^2 = 0.777$ and $R = 0.882$, respectively).

$$\begin{aligned}
 pKi = & 87.623 - 193.402 \times D + 11.223 \times \%H + 1.393 \\
 & \times VDWE - 0.048 \times TE - 1.080 \times \%N - 0.479 \times \%O \\
 & + 80.55646 \times D^2 - 0.866 \times \%H^2 - 0.027 \\
 & \times VDWE^2 - 0.00038 \times TE^2 + 0.014 \times \%N^2 - 0.004 \\
 & \times \%O^2
 \end{aligned} \quad (2)$$

3.3. Validation of predictive QSAR models

3.3.1. External validation

External validation is an essential and critical step to examine the reliability of MLR and MNL QSAR models, ensuring their application to new molecules included in the test set (Rezende et al., 2019). Based on developed models in equations (1) and (2) for twenty-four molecules (training set), we tested six novel molecules (2, 10, 11, 13, 19, 24) which are part of test set, and we obtained an external correlation coefficient of $R^2_{ext} = 0.648$ and $R^2_{ext'} = 0.872$ for MLR and MNL models, respectively. According to Golbreikh and Tropsha's study, the linear and non-linear models are externally validated because the external correlation coefficients are superior to 0.6. The Table 3, shows the predicted activities for six novel molecules by MLR and MNL models, where the quantitative correlations are translated in Figs. 2 and 3, successively.

3.3.2. Internal validation

A cross-validation (CV) technique was performed using the leave-one-out (LOO) procedure, for internal validation of the established QSAR models, testing each chemical compound once, modeling a new mathematical model on twenty-three molecules each time ($N-1 = 23$) and predicting human GluT1

Table 2 Analysis of variance using the fisher test.

Source	DDL	Total square	Mean square	F	Pr > F
Model	6	14.923	2.487	8.332	0.000
Error	17	5.075	0.299		
Adjusted total	23	19.998			

Table 3 The observed and predicted activities of pKi order using MLR and MNLN models.

Compounds number	Molecules nomenclature	Observed pKi	Predicted pKi (MLR)	Predicted pKi (MNLN)
2*	(3R,4S)-1-((1-methyl-1H-imidazol-4-yl)sulfonyl)-N,4-diphenylpyrrolidin-3-amine.	6.701	5.447	5.606
10*	N-((3R,4S)-4-(4-fluorophenyl)-1-((1-methyl-1H-imidazol-4-yl)sulfonyl)pyrrolidin-3-yl)-5-(trifluoromethyl)pyridin-3-amine.	5.936	7.218	7.088
11*	(3R,4S)-N-(3-chlorophenyl)-4-(3-fluorophenyl)-1-((1-methyl-1H-imidazol-4-yl)sulfonyl)pyrrolidin-3-amine.	7.377	8.286	8.257
13*	N-((3R,4S)-4-(4-fluorophenyl)-1-((1-methyl-1H-imidazol-4-yl)sulfonyl)pyrrolidin-3-yl)-2-(trifluoromethyl)pyridin-4-amine.	6.928	7.986	7.870
19*	(3R,4S)-N-((R)-2,3-dihydro-1H-inden-1-yl)-4-(4-fluorophenyl)-1-((1-methyl-1H-imidazol-4-yl)sulfonyl)pyrrolidin-3-amine.	9.000	10.644	9.518
24*	4-(((3R,4S)-3-benzyl-4-phenylpyrrolidin-1-yl)sulfonyl)-1-methyl-1H-imidazole.	7.032	6.653	7.845

* Indicates the test set molecules.

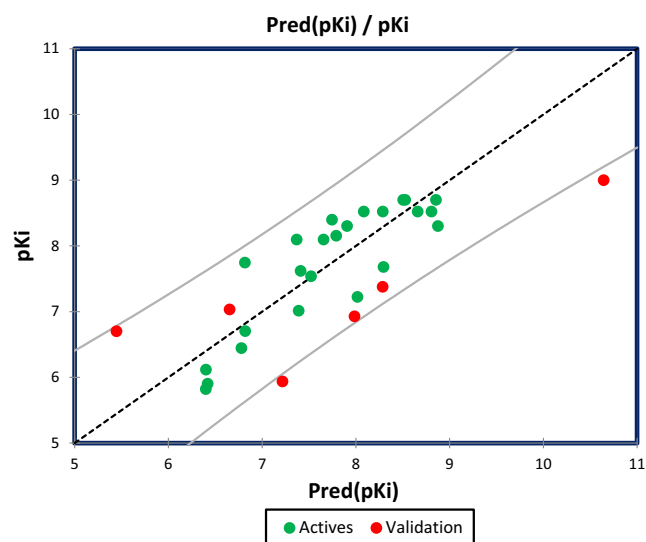


Fig. 2 Quantitative correlation between observed and predicted GluT1 activity using MLR technique.

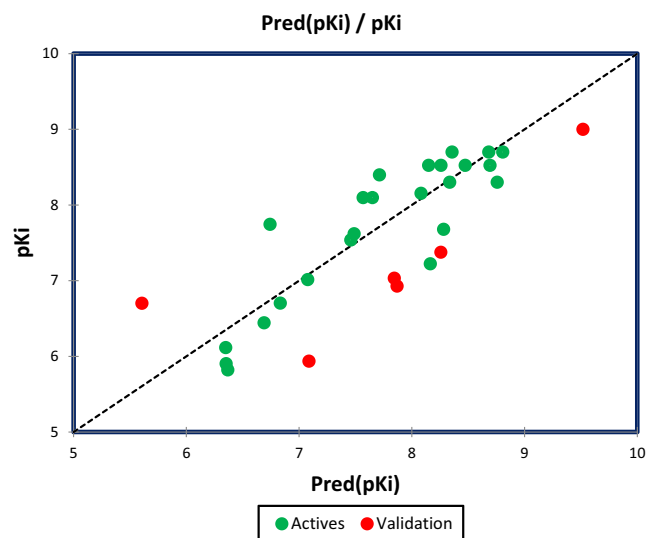


Fig. 3 Quantitative correlation between observed and predicted GluT1 activity using MNLN technique.

activity for each tested molecule (Rafało, 2022). The process was repeated for all molecules in the training set, as resulted in Table 4. Afterwards, the quadratic coefficient (Q^2_{cv}) of cross-validation, was calculated based on the following equation:

$$Q^2_{cv} = 1 - \frac{\sum_i^n (Y_{ob} - Y_{pr})^2}{\sum_i^n (Y_{ob} - Y_{mean})^2} \text{Equation3(Elfadilietal., 2023)}$$

As: Y_{ob} : the observed activity, Y_{pr} : the predicted activity, and Y_{mean} : the mean of observed activities.

According to Golbreikh and Tropsha's study, although the result of quadratic coefficient ($Q^2_{cv} = 0.546$) exceeds 0.5, so the developed QSAR model is internally validated with a good reliability and strong predictivity.

Table 4.

3.3.3. Validation using Y-randomisation test

According to Golbreikh and Tropsha's study, the highest value of quadratic coefficient generated by cross validation technique with the leave one out procedure (CVLOO) is probable to be overestimated and may refers to a lucky correlation, so the internal validation is necessary but still not enough sufficient. For this reason, the Y-Randomization test is so required (Golbraikh and Tropsha, 2002; Halder and Jha, 2010). Using java Platform SE binary, we evaluated the predictive accuracy of developed QSAR model through one hundred randomizations as resulted in Table S4. The value of cR^2_p criteria was 0.621, which exceeds 0.5 threshold. Moreover, the resulted correlation, determination, and cross-validation with the leave-one-out procedure coefficients of the original model are so higher than the marked values for all 100 randomizations. So, the predicted GlyT1 activity by the originally developed model are not due to random chance.

3.3.4. Statistical criterias of Golbreikh and Tropsha's study

Golbreikh and Tropsha's statistical study emphasizes that a certain number of postulated conditions must be verified before the quantitative structure-activity relationship model can be applied to other new molecules. In this part, we noted that the generated model by MLR technique satisfy with success all postulated threshold conditions of Tropsha and Golbraikh's theory, as presented in Table 5. Consequently, the developed model is qualified by an accurate and precise predic-

Table 4 The observed and predicted activities using MLR, MNLR and CVLOO techniques.

Molecules number	Molecules nomenclature	Observed pKi	Predicted pKi (MLR)	Predicted pKi (MNLR)	Predicted pKi (CVLOO)
1	2-chloro-N-((3R,4S)-1-((1-methyl-1H-imidazol-4-yl)sulfonyl)-4-phenylpyrrolidin-3-yl)-3-(trifluoromethyl)benzamide.	6.703	6.820	6.834	7.131
3	(3R,4S)-1-((1-methyl-1H-imidazol-4-yl)sulfonyl)-4-phenyl-N-(o-tolyl)pyrrolidin-3-amine.	5.821	6.399	6.367	6.648
4	(3R,4S)-1-((1-methyl-1H-imidazol-4-yl)sulfonyl)-4-phenyl-N-(m-tolyl)pyrrolidin-3-amine.	7.745	6.817	6,742	6.417
5	(3R,4S)-1-((1-methyl-1H-imidazol-4-yl)sulfonyl)-4-phenyl-N-(p-tolyl)pyrrolidin-3-amine.	5.903	6.419	6.353	6.634
6	(3R,4S)-1-((1-methyl-1H-imidazol-4-yl)sulfonyl)-4-phenyl-N-(3-(trifluoromethyl)phenyl)pyrrolidin-3-amine.	8.097	7.370	7.651	7.292
7	(3R,4S)-4-(4-fluorophenyl)-1-((1-methyl-1H-imidazol-4-yl)sulfonyl)-N-(3-(trifluoromethyl)phenyl)pyrrolidin-3-amine.	8.523	8.085	8.150	8.018
8	(3R,4S)-N-(3-chlorophenyl)-4-(4-fluorophenyl)-1-((1-methyl-1H-imidazol-4-yl)sulfonyl)pyrrolidin-3-amine.	8.523	8.288	8.259	8.247
9	(3R,4S)-N-(4-fluoro-3-(trifluoromethyl)phenyl)-4-(4-fluorophenyl)-1-((1-methyl-1H-imidazol-4-yl)sulfonyl)pyrrolidin-3-amine.	8.301	8.876	8.758	9.085
12	(3R,4S)-N-(3-chlorophenyl)-4-(2-fluorophenyl)-1-((1-methyl-1H-imidazol-4-yl)sulfonyl)pyrrolidin-3-amine.	7.678	8.296	8.282	8.394
14	(3R,4S)-1-((1-methyl-1H-imidazol-4-yl)sulfonyl)-4-(pyridin-3-yl)-N-(3-(trifluoromethyl)phenyl)pyrrolidin-3-amine.	6.116	6.401	6.350	6.494
15	(3R,4S)-4-(4-fluorophenyl)-1-((1-methyl-1H-imidazol-4-yl)sulfonyl)-N-(3-(trifluoromethoxy)phenyl)pyrrolidin-3-amine.	8.398	7.745	7.714	7.639
16	N-((3R,4S)-4-(4-fluorophenyl)-1-((1-methyl-1H-imidazol-4-yl)sulfonyl)pyrrolidin-3-yl)-4-(trifluoromethyl)pyridin-2-amine.	8.097	7.656	7.568	7.576
17	N-((3R,4S)-4-(4-fluorophenyl)-1-((1-methyl-1H-imidazol-4-yl)sulfonyl)pyrrolidin-3-yl)-6-(trifluoromethyl)pyrimidin-4-amine.	8.301	7.906	8.337	7.629
18	(3R,4S)-N-(4-fluoro-3-(trifluoromethoxy)phenyl)-4-(4-fluorophenyl)-1-((1-methyl-1H-imidazol-4-yl)sulfonyl)pyrrolidin-3-amine.	8.699	8.504	8.357	8.477
20	(3R,4S)-N-(4-fluoro-3-(trifluoromethyl)phenyl)-4-(4-fluorophenyl)-1-((1-methyl-1H-1,2,3-triazol-4-yl)sulfonyl)pyrrolidin-3-amine.	8.523	8.806	8.694	8.896
21	4-(((3S,4R)-3-(4-fluorophenyl)-4-((3-(trifluoromethoxy)phenoxy)methyl)pyrrolidin-1-yl)sulfonyl)-1-methyl-1H-imidazole.	8.155	7.790	8.082	7.649
22	((3R,4S)-4-(4-fluorophenyl)-1-((1-methyl-1H-imidazol-4-yl)sulfonyl)pyrrolidin-3-yl)(3-(trifluoromethoxy)phenyl)methanone.	7.538	7.522	7.459	7.515
23	N-(((3S,4S)-4-(4-fluorophenyl)-1-((1-methyl-1H-imidazol-4-yl)sulfonyl)pyrrolidin-3-yl)methyl)-3-(trifluoromethoxy)aniline.	7.222	8.017	8.164	8.108
25	4-(((3R,4S)-4-(4-fluorophenyl)-1-((1-methyl-1H-imidazol-4-yl)sulfonyl)pyrrolidin-3-yl)oxy)-6-(trifluoromethyl)pyrimidine.	7.013	7.390	7.077	7.583
26	(3R,4S)-4-(4-fluorophenyl)-1-((1-methyl-1H-imidazol-4-yl)sulfonyl)-N-(3-(trifluoromethoxy)phenyl)pyrrolidine-3-carboxamide.	6.444	6.779	6.690	7.137
27	(3R,4R)-1-((1-methyl-1H-imidazol-4-yl)sulfonyl)-4-((R)-tetrahydro-2H-pyran-2-yl)-N-(3-(trifluoromethoxy)phenyl)pyrrolidine-3-carboxamide.	8.523	8.660	8.474	8.714
28	(3R,4R)-1-((1-methyl-1H-imidazol-4-yl)sulfonyl)-4-((S)-tetrahydrofuran-2-yl)-N-(3-(trifluoromethoxy)phenyl)pyrrolidine-3-carboxamide.	7.620	7.411	7.489	6.921
29	(3R,4R)-4-(1,3-dioxepan-2-yl)-1-((1-methyl-1H-imidazol-4-yl)sulfonyl)-N-(3-(trifluoromethoxy)phenyl)pyrrolidine-3-carboxamide.	8.699	8.854	8.806	8.968
30	(3R,4R)-4-(1,3-dioxan-2-yl)-1-((1-methyl-1H-imidazol-4-yl)sulfonyl)-N-(3-(trifluoromethoxy)phenyl)pyrrolidine-3-carboxamide.	8.699	8.527	8.682	8.445

tivity, which affirms again that human GlyT1 activity is really affected by the six selected descriptors.

3.4. In-silico pharmacokinetics ADMET prediction

We initiated the in-silico screening of thirty human GlyT1 inhibitors, using the BOILED-Egg model as a widely applied predictive technique in the field of medicinal chemistry, to

discover drug candidates that could penetrate the central nervous system (CNS), as resulted in Fig. 4. We noticed that most of the chemical compounds are part of white Egan Eggs, so they are predicted to be absorbed by the gastrointestinal tract, except the molecules marked as 2, 3, 4, 5, and 19, which are part of the yellow part of Egan-egg, thus they are predicted to be effluated from the central nervous system (CNS) by the P-glycoprotein, and predicted as potent inhibitors with an

Table 5 Tropsha and Golbraikh conditions to examine the accuracy of generated MLR QSAR model.

Statistical parameters	Developed Equations	Model scores	Threshold	Comment
R^2	$R^2 = 1 - \frac{\sum (Y_{obs} - Y_{cal})^2}{\sum (Y_{obs} - \bar{Y}_{obs})^2}$	0.746	> 0.6	Accepted
R^2_{adj}	$R^2_{adj} = \frac{(N-1)R^2 - p}{N-p-1}$	0.657	> 0.6	Accepted
R^2_{test}	$R^2_{test} = 1 - \frac{\sum Y_{cal(test)} - Y_{obs(test)}^2}{\sum (Y_{obs(test)} - \bar{Y}_{obs(train)})^2}$	0.648	> 0.6	Accepted
Q^2_{cv}	$Q^2_{cv} = 1 - \frac{\sum (Y_{cal} - Y_{obs})^2}{\sum (Y_{obs} - \bar{Y}_{obs})^2}$	0.529	> 0.5	Accepted
R^2_{rand}	The average of 100 R2rand (i)	0.243	< R^2	Accepted
Q^2_{cv} 'LOO' rand	The average for 100 Q^2_{cv} 'LOO' rand (i)	-0.660	< Q^2_{cv}	Accepted
cR^2_p	$cR^2_p = R^2 - (Average R_{rand})^2$	0.621	> 0.5	Accepted

important ability to cross the blood–brain barrier (BBB). However, molecule 24 colored in red was predicted to not be effluated from the central nervous system, but it's capable to pass through the blood–brain barrier (BBB) (Daina and Zoete, 2016). Therefore, we conclude that just five glycine transporter type 1 inhibitors (C2, C3, C4, C5, and C19) which are predicted as central nervous system agents with the highest probability to cross the blood–brain barrier.

Subsequently, we studied the physicochemical and pharmacokinetic properties of all central nervous system agents, as shown in Table 6 and Table 7, respectively. Based on the properties of nortriptyline as a positive control molecule co-crystallized with the DAT protein, we noticed that all predicted inhibitors are in good agreement with nortriptyline, where they respect all five rules of Lipinski ($MW \leq 500$ g/mol, $40 \leq MR \leq 130$, $HBD < 5$, $\text{Log P (Octanol/Water)} < 5$,

$HBA \leq 10$) (Er-raiy et al., 2022; Er-raiy et al., 2023a; Er-raiy et al., 2023b), and satisfy the violations number of Veber, Ghose, Egan, and Muegge (Jia et al., 2020). Moreover, the pharmacokinetics properties reveal a good ADME-Toxicity profile, where all predicted molecules are defined by a good human intestinal absorption (HIA superior than 94 %), and the values of CNC and BBB permeabilities are included in (-2 to -3) Log PS, and higher than -1 Log BB, respectively. Thus, they have a good permeabilities to the central nervous system (CNS) and the blood–brain barrier (BBB). In addition, they are all predicted as substrates of 3A4 cytochrome. C4 and C24 compounds and C19 as the most active ligand, are predicted as potent inhibitors for 2C9 and 3A4 cytochromes. Also, they are defined by an excretion of a total clearance inferior than 1 Log ml/min/kg. According to the AMES toxicity test, all chemical compounds are predicted as non-toxic inhibi-

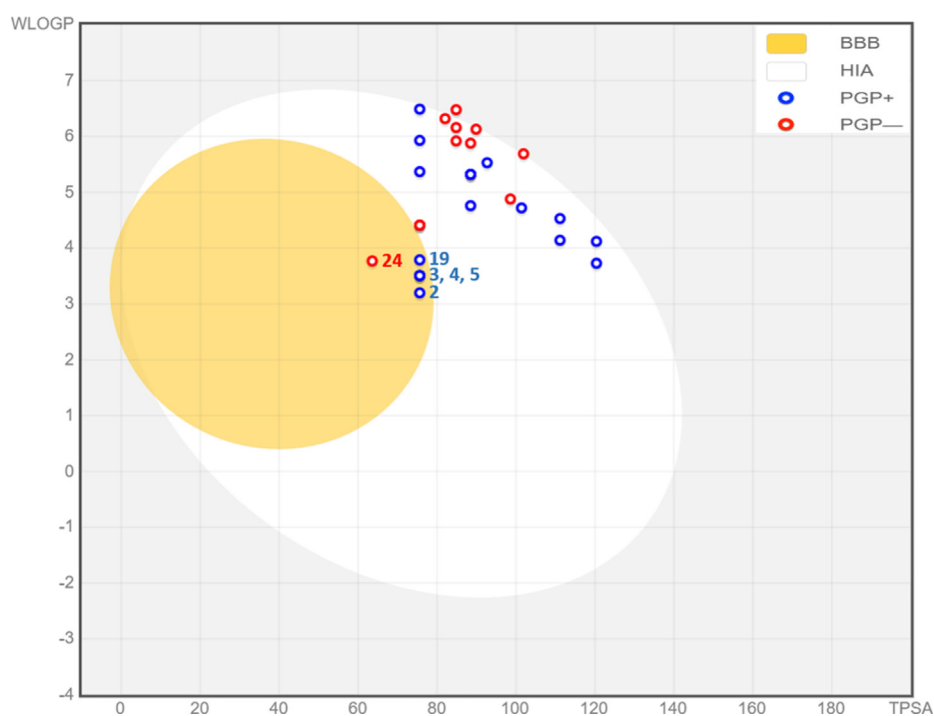
**Fig. 4** The predictive model of BOILED-Egg for 3,4-disubstituted pyrrolidine.

Table 6 Prediction of physico-chemical parameters of central nervous system agents.

Compounds number	Physical and chemical properties						Lipinski violations	Veber violations	Egan violations	Ghose violations	Muegge violations
	Molecular weight (g/mol)	Molar refractive index	Rotatable bonds Number	Log P (Octanol/Water)	H-bond Acceptors Number	H-bond donors Number	Categorical (Yes/No)				
Threshold	≤ 500	40 ≤ MR ≤ 130	< 10	< 5	≤ 10	< 5					
C2	382.48	109.01	5	3.03	4	1	Yes	Yes	Yes	Yes	Yes
C3	396.51	113.98	5	2.65	4	1	Yes	Yes	Yes	Yes	Yes
C4	396.51	113.98	5	3.24	4	1	Yes	Yes	Yes	Yes	Yes
C5	396.51	113.98	5	3.00	4	1	Yes	Yes	Yes	Yes	Yes
C19	440.53	119.90	5	3.37	6	1	Yes	Yes	Yes	Yes	Yes
C24	381.49	109.48	5	2.55	4	0	Yes	Yes	Yes	Yes	Yes
Nortriptylene	263.38	86.06	3	3.22	1	1	Yes	Yes	Yes	Yes	No

Table 7 Prediction of ADMET-Toxicity pharmacokinetic properties of central nervous system agents.

Compounds number	Absorption	Distribution		Metabolism						Excretion	Toxicity			
	Intestinal Absorption (human)	BBB permeability	CNS permeability	Substrate			Inhibitor			Total Clearance	AMES Toxicity	Hepatotoxicity	Skin Sensitization	
				Cytochromes										
				2D6	3A4	1A2	2C19	2C9	2D6	3A4				
	Numeric (% Absorbed)	Numeric (Log BB)	Numeric (Log PS)	Categorical (Yes/No)						Numeric (Log ml/min/kg)	Categorical (Yes/No)			
C2	94.986	0.175	-2.334	No	Yes	No	Yes	Yes	No	No	0.27	Not toxic	Yes	No
C3	96.126	0.219	-2.264	No	Yes	No	Yes	No	No	Yes	0.269	Not toxic	Yes	No
C4	95.608	0.142	-2.254	No	Yes	No	Yes	Yes	No	Yes	0.264	Not toxic	Yes	No
C5	95.522	0.125	-2.26	No	Yes	No	Yes	No	No	Yes	0.272	Not toxic	Yes	No
C19	94.049	0.151	-2.313	No	Yes	No	No	Yes	No	Yes	0.41	Not toxic	Yes	No
C24	99.251	0.066	-2.216	No	Yes	Yes	Yes	Yes	No	Yes	0.114	Not toxic	Yes	No
Nortriptylene	97.482	0.808	-1.196	No	Yes	Yes	No	No	Yes	No	0.929	Not toxic	Yes	Yes

tors of the human body, without any skin sensitization, but they have a known positive hepatotoxicity.

3.5. Molecular docking

The results of molecular docking simulation exposed in the Fig. 5, demonstrate the intermolecular interactions produced between the dopamine transporter (DAT) protein as a key therapeutic strategy to treat clinical depression and neuropathic pain (Adamski et al., 2017; Belhassan et al., 2019), and the compound C19 as the most active ligand with a good ADME-Toxicity profile. 2D and 3D dimensional visualizations confirm that C19 ligand forms two hydrogen bonds towards ASP 475 and GLU 480 amino acids residues of DAT protein in A chain, with nuclear distances of 3.90 Å and 3.07 Å respectively, taking into account that the chemical bonds of the hydrogen bonding type make the (ligand-protein) complex so stable. Additionally, C19 reacts to VAL 120 and ALA 479 amino acids forming two chemical bonds of Pi-Alkyl type at 6.08 Å and 3.95 Å, respectively. And Pi-Pi T-shaped bond with TYR 124 amino acid at 5.39 Å. Consequently, ASP 475, GLU 487, VAL 120, ALA 479, and TYR 124 are the main sites of glycine transporter type 1 inhibition for the candidate drug. The resulted chemical bonds include intermolecular interactions similar to those detected towards Tyr 124, Ala 479, and Val 120 amino acid residues, which have

been produced by two selective GluT1 inhibitors, after being bound to the same membrane protein of drosophila melanogaster dopamine transporter (DAT), which were also designed to improve memory performance while treating depression and the cognitive symptoms associated with schizophrenia (El fadili et al., 2023; Hudson et al., 2020; Santora et al., 2018).

3.6. Docking validation protocol

The process of molecular docking simulations was examined using docking validation protocol or re-docking methodology for the (C19 ligand – DAT protein) complex. In the first time, we have compared the intermolecular interactions produced for the studied complex with the active sites of nortriptyline as co-crystallized ligand bound to the same chain of targeted protein. Where, the active sites of nortriptyline are the residues of TYR 124, PHE 325, and PHE 43 amino acids, which are experimentally extracted using the ProteinsPlus online server (“Zentrum für Bioinformatik: Universität Hamburg - Proteins Plus Server,” n.d.), as resulted in Fig. 6A, and TYR 124, PHE 325, PHE 43, VAL 120, and ALA 479 amino acids, which are theoretically produced using Autodock tools, as presented in Fig. 6B. Therefore, we noticed that TYR 124, VAL 120, and ALA 479 amino acids are the same amino acids, which were obtained for (C19 - DAT protein) complex. In second time, we have used the superposition

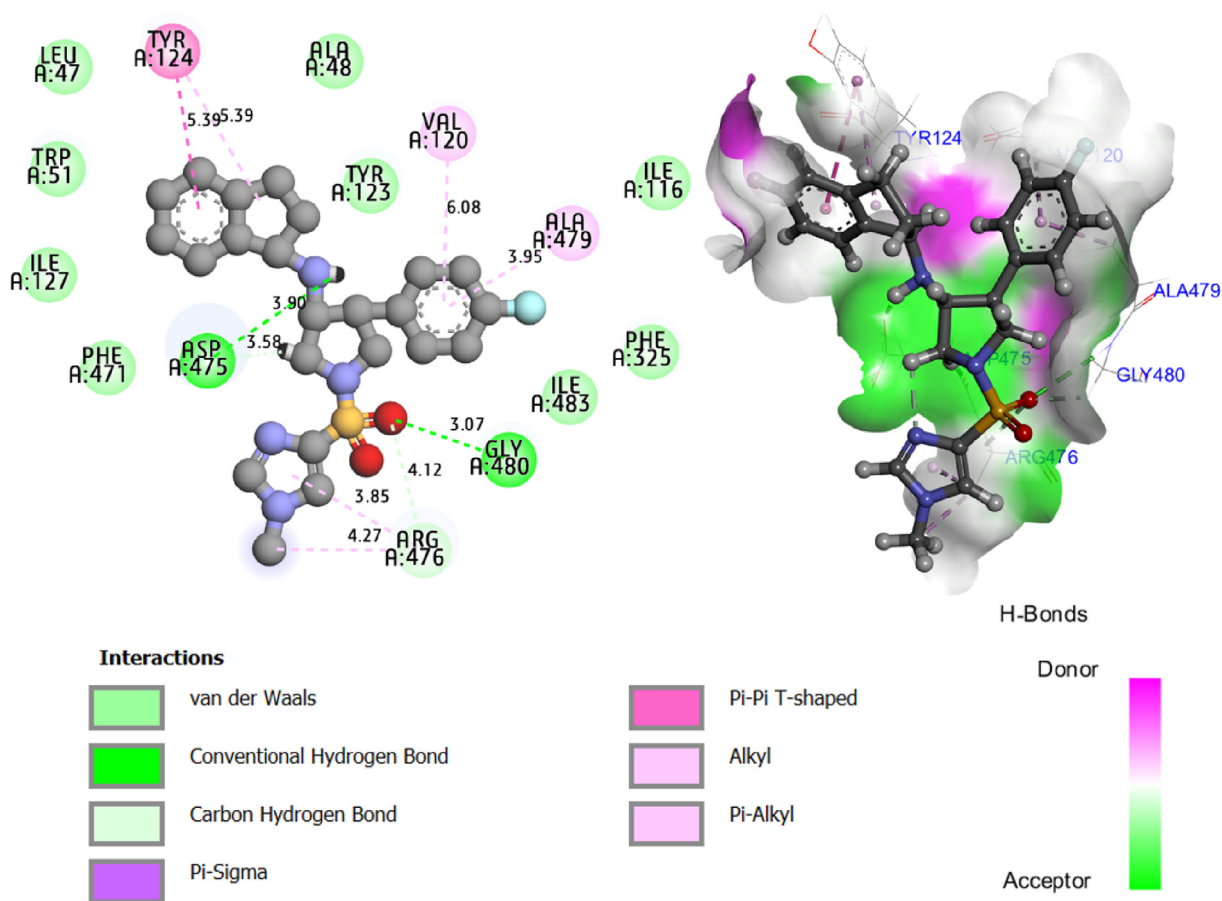


Fig. 5 2D (left) and 3D (right) intermolecular interactions, produced for (C19 ligand - DAT protein) complex with binding energy of -8.96 Kcal/mol.

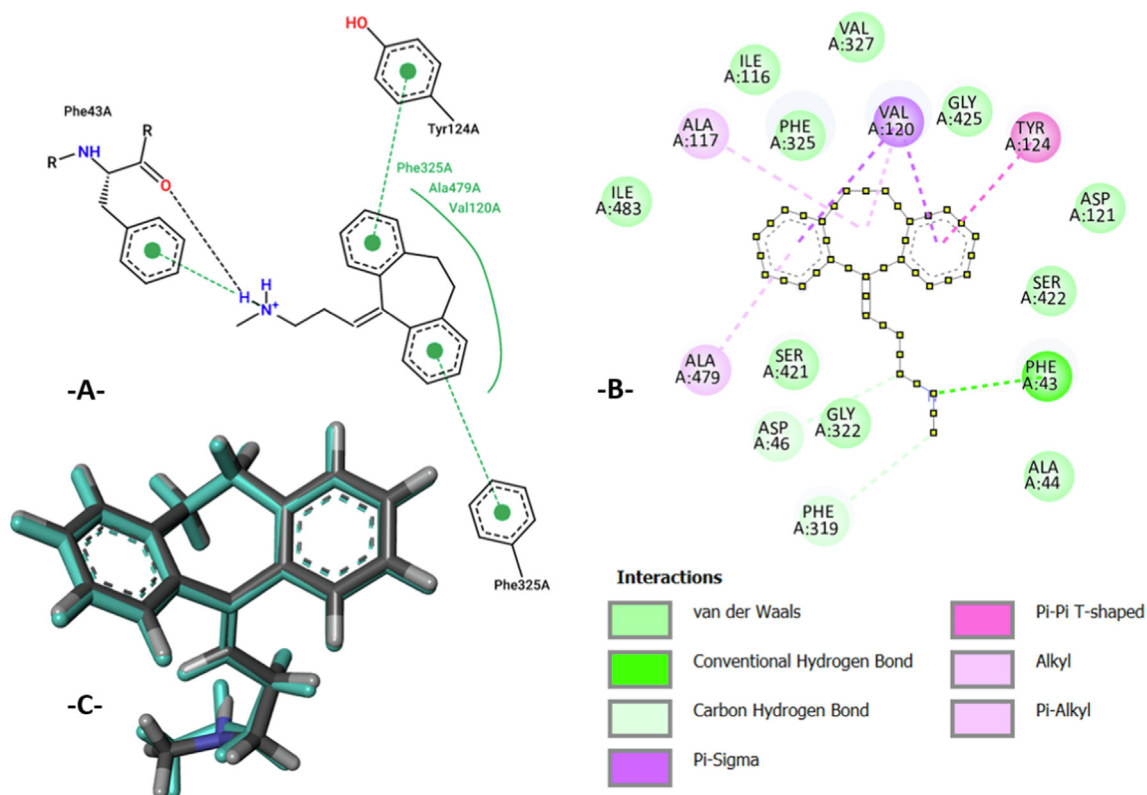


Fig. 6 The active sites of co-crystallized ligand of DAT protein in A-chain. B: 2D intermolecular interactions produced for the (docked nortriptyline - DAT protein) complex with a binding energy of -9.02 kcal/mol. C: Re-docking pose with a RMSD value of 0.128 Å (co-crystallized nortriptyline colored in cyan superposed on docked nortriptyline).

of co-crystallized and docked nortriptyline, and we have obtained a good overlay pose with a minimal root mean square deviation (RMSD = 0.128) which is <2 Å as shown in Fig. 6C. Therefore, we conclude that the candidate drug was docked in the active sites of targeted protein, and the process of molecular docking is successfully validated (Abdullahi et al., 2020).

3.7. Molecular dynamic simulation

High-performance molecular dynamics simulation was performed to study the stability of intermolecular interactions

produced for the (C19 ligand - DAT protein) complex during 100 ns (El fadili et al., 2022b; Er-rajy et al., 2023). The results of the conformational changes presented in Fig. 7 show that the root mean square deviation (RMSD) of the candidate ligand oscillates in parallel with the RMSD values of the protein target during the first thirty nanoseconds, then destabilizes a little, and stabilizes again during the last thirty nanoseconds due to the effect of heavy atoms as oxygen and nitrogen which make the ligand-protein complex so stable. In addition, there are no deviations greater than 3 Å, which demonstrates that the simulation remains in equilibrium during the molecular dynamics simulation time without any noticeable deviation.

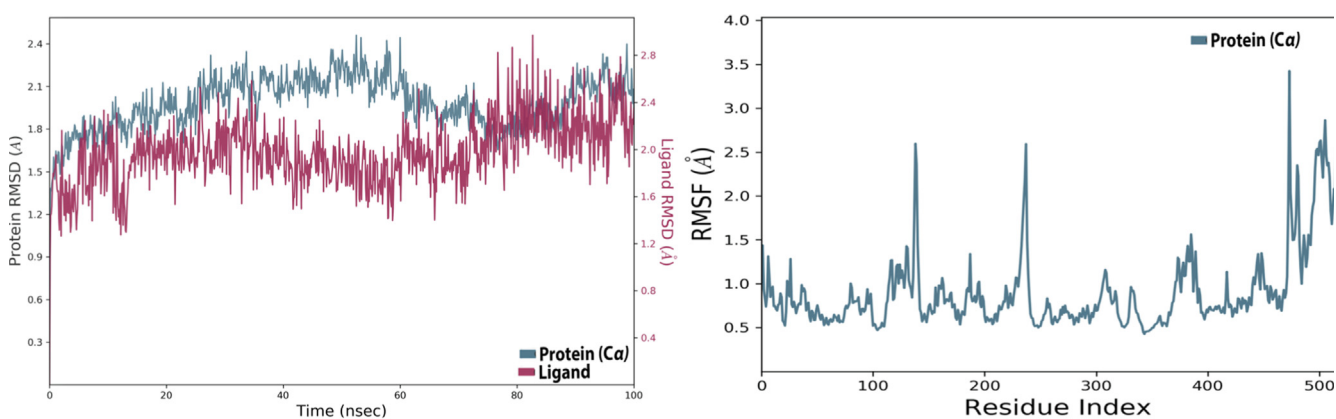


Fig. 7 The changes of Root Mean Square Deviation (RMSD) and Root Mean Square Fluctuation (RMSF) during 100 ns, for the dopamine transporter protein complexed with C19 ligand.

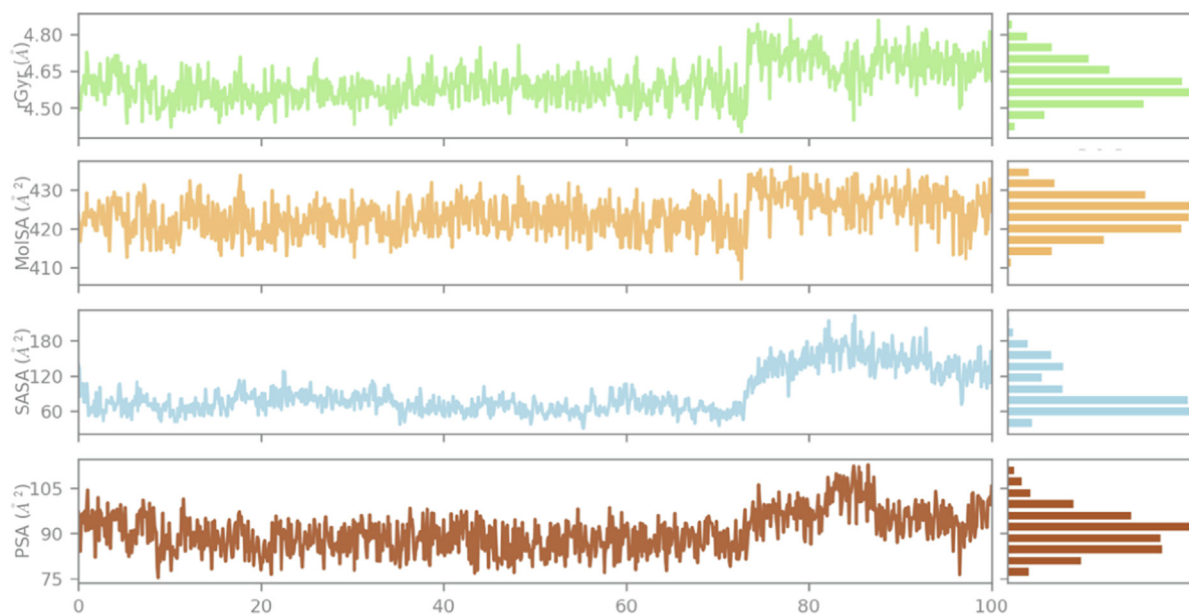


Fig. 8 The changes in radius of gyration (r_{Gyr}), molecular surface area (MolSA), solvent accessible surface area (SASA), and polar surface area (PSA), over 100 ns of molecular dynamics simulation time.

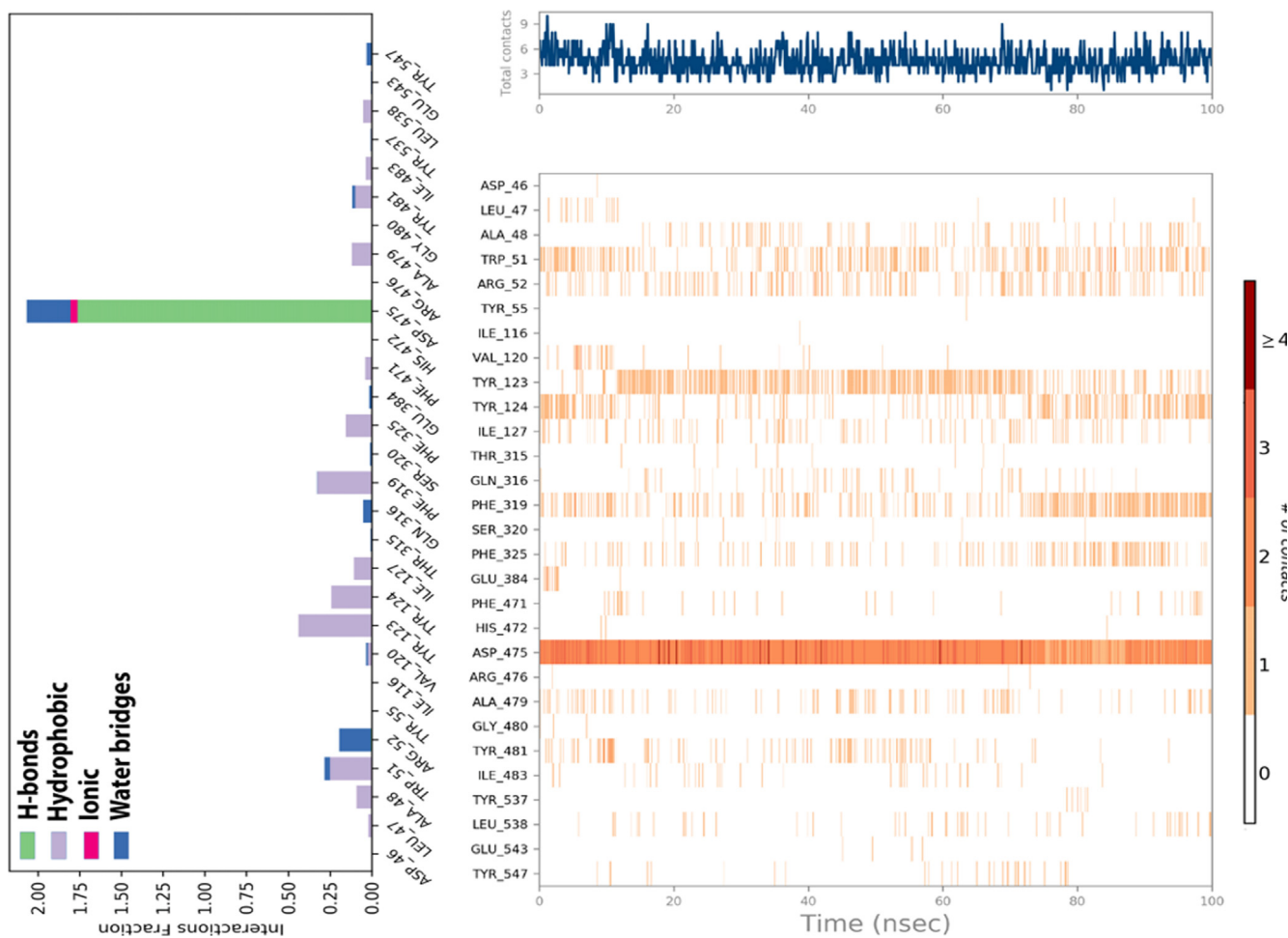


Fig. 9 The histogram of interaction fractions between DAT protein and C19 ligand (left), and the timeline depiction of intermolecular interactions and chemical contacts of candidate ligand in the active sites of targeted protein (right).

Table 8 Binding energies in Kcal/mol of the studied complex using MMGBSA approach.

Studied complex	MMGBSA dG Bind	MMGBSA dG Bind Coulomb	MMGBSA dG Bind Covalent	MMGBSA dG Bind Hbond	MMGBSA dG Bind Lipo	MMGBSA dG Bind Solv GB	MMGBSA dG Bind vdW
(C19 – protein) complex	–51.417899	–56.518147	1.557139	–0.820922	–23.877425	73.360626	–45.119169

Secondly, the root mean square fluctuation (RMSF) values show only two remarkable fluctuations for the residuals 470 and 530, which exceeded 3 Å, as shown in Fig. 7. So, we conclude that the ligand does not diffuse far from its primary binding site.

In addition, we recorded negligible fluctuations for ligand properties, such as radius of gyration (r Gyr), molecular surface area (MolSA), solvent accessible surface area (SASA), and polar surface area (PSA), which all oscillate in a very small range over 75 ns, making just one remarkable fluctuation at the same time, due to the influence of nitrogen, oxygen, sulfur, and fluorine, as typical heteroatoms characterizing this organic molecule (AlAmiery, 2023; TANWER and Shukla, 2023). However, they stabilize again until the rest of the molecular dynamics simulation time as displayed in Fig. 8, which demonstrates minimal changes in the compactness of the candidate ligand. Consequently, the targeted protein is very flexible after being bound to the candidate ligand.

Furthermore, the upper panel shown in Fig. 9, reflects the specified number of contacts produced by the candidate ligand towards the targeted protein throughout molecular dynamics simulation time, while the lower panel displays the residues of amino acids, which reacted with the C19 compound along the trajectory. The scale on the right-hand side of the graph shows that the strongest connection is one that corresponds to a dark orange residue that has entered into more than one chemical reaction with the candidate ligand (Ebenezer et al., 2022). For this, ASP 475 amino acid residue has the main function in the stability of (protein–ligand) complex throughout 100 ns of MD simulation time, which presents an important interaction fraction of H-bonds as displayed on the left side of Fig. 9.

The Molecular Mechanics with Generalized Born and Surface Area (MMGBSA) solvation was equally conducted to calculate the binding free energies of the C19 ligand in complex with DAT protein, as resulted in Table 8 (Faisal et al., 2022; Ononamadu et al., 2021). The MMGBSA approach shows that the binding energies are negatively very large, indicating that the candidate drug have reacted with the protein target with low energies (minimal ΔG Bind scores), which makes the complex so stable with optimal energies during the molecular dynamic's simulation time.

4. Conclusion

In summary, quantitative structure–activity relationships reveal that constitutional and geometric descriptors have a key function in the human GluT1 activity of the 3,4-disubstituted pyrrolidine sulfonamides family. In-silico screening indicates that C2, C3, C4, C5, and C19 were predicted as non-toxic inhibitors of the human body, and functioning as central nervous system agents with the highest probability to cross the blood–brain barrier, respecting Lipinski, Veber, Egan, Muegge, and Rhose conditions. The compound C19 having the highest

activity and predicted with a good ADME-Tox profile, was chosen for molecular docking and molecular dynamics simulations, which indicate that this candidate ligand produced stable intermolecular interactions with ASP 475, GLU 480, VAL 120, ALA 479, and TYR 124 amino acids residues of dopamine transporter protein, because the studied properties of (C19 ligand – DAT protein) complex remained perfectly stable until 100 ns of molecular dynamic simulation time with lowest binding energies of MMGBSA solvation. Therefore, C19 ligand is strongly recommended as candidate drug to treat schizophrenia and similar disabilities in relation with glutaminergic N-methyl-D-aspartate receptor hypofunction.

Declaration of Competing Interest

The authors declare that they have no known competing financial interests or personal relationships that could have appeared to influence the work reported in this paper.

Funding

This research was funded by Princess Nourah bint Abdulrahman University Researchers Supporting Project number (PNURSP2023R141), Princess Nourah bint Abdulrahman University, Riyadh, Saudi Arabia.

Acknowledgment

The authors extend their appreciation to Princess Nourah bint Abdulrahman University Researchers Supporting Project number (PNURSP2023R141), Princess Nourah bint Abdulrahman University, Riyadh, Saudi Arabia.

Appendix A. Supplementary material

Supplementary data to this article can be found online at <https://doi.org/10.1016/j.arabjc.2023.105105>.

References

- Abdullahi, M., Shallangwa, G.A., Uzairu, A., 2020. In silico QSAR and molecular docking simulation of some novel aryl sulfonamide derivatives as inhibitors of H5N1 influenza A virus subtype. Beni-Suef Univ. J. Basic Appl. Sci. 9, 2. <https://doi.org/10.1186/s43088-019-0023-y>.
- Adamski, A., Kruszka, D., Dutkiewicz, Z., Kubicki, M., Gorczyński, A., Patroniak, V., 2017. Novel family of fused tricyclic [1,4]diazepines: Design, synthesis, crystal structures and molecular docking studies. Tetrahedron 73, 3377–3386. <https://doi.org/10.1016/j.tet.2017.05.015>.
- AlAmiery, A., 2023. Gravimetric and Density Functional Theory Investigations on 4-Amioantipyrin Schiff base as an inhibitor for mild steel in HCl solution. Prog. Color Colorants Coat. <https://doi.org/10.30509/pccc.2023.167077.1196>

- Alberati, D., Moreau, J.-L., Lengyel, J., Hauser, N., Mory, R., Borroni, E., Pinard, E., Knoflach, F., Schlotterbeck, G., Hainzl, D., Wettstein, J.G., 2012. Glycine reuptake inhibitor RG1678: A pharmacologic characterization of an investigational agent for the treatment of schizophrenia. *Neuropharmacology* 62, 1152–1161. <https://doi.org/10.1016/j.neuropharm.2011.11.008>.
- Amberg, W., Lange, U.E.W., Ochse, M., Pohlki, F., Behl, B., Relo, A. L., Hornberger, W., Hoft, C., Mezler, M., Sydor, J., Wang, Y., Zhao, H., Brewer, J.T., Dietrich, J., Li, H., Akritopoulou-Zanze, I., Lao, Y., Hannick, S.M., Ku, Y.-Y., Vasudevan, A., 2018. Discovery of novel aminotetralines and aminochromanes as selective and competitive glycine transporter 1 (GlyT1) inhibitors. *J. Med. Chem.* 61, 7503–7524. <https://doi.org/10.1021/acs.jmedchem.8b00300>.
- Atkinson, B.N., Bell, S.C., De Vivo, M., Kowalski, L.R., Lechner, S. M., Ognyanov, V.I., Tham, C.-S., Tsai, C., Jia, J., Ashton, D., Klitenick, M.A., 2001. ALX 5407: A potent, selective inhibitor of the hGlyT1 glycine transporter. *Mol. Pharmacol.* 60, 1414–1420. <https://doi.org/10.1124/mol.60.6.1414>.
- Bank, R.P.D., n.d. RCSB PDB - 4M48: X-ray structure of dopamine transporter elucidates antidepressant mechanism [WWW Document]. URL <https://www.rcsb.org/structure/4M48> (accessed 1.6.23a).
- Bassani, D., Pavan, M., Bolcato, G., Sturlese, M., Moro, S., 2022. Re-exploring the ability of common docking programs to correctly reproduce the binding modes of non-covalent inhibitors of SARS-CoV-2 Protease Mpro. *Pharmaceuticals* 15, 180. <https://doi.org/10.3390/ph15020180>.
- Bastianoni, A., Guastaldi, E., Barbagli, A., Bernardinetti, S., Zirulia, A., Brancale, M., Colonna, T., 2021. Multivariate analysis applied to aquifer hydrogeochemical evaluation: A case study in the coastal significant subterranean water body between “Cecina River and San Vincenzo”, Tuscany (Italy). *Appl. Sci.* 11, 7595. <https://doi.org/10.3390/app11167595>.
- Belhassan, A., Zaki, H., Benlyas, M., Lakhli, T., Bouachrine, M., 2019. Study of novel triazolo-benzodiazepine analogues as antidepressants targeting by molecular docking and ADMET properties prediction. *Heliyon* 5, e02446.
- Blackaby, W.P., Lewis, R.T., Thomson, J.L., Jennings, A.S.R., Goodacre, S.C., Street, L.J., MacLeod, A.M., Pike, A., Wood, S., Thomas, S., Brown, T.A., Smith, A., Pillai, G., Almond, S., Guscott, M.R., Burns, H.D., Eng, W., Ryan, C., Cook, J., Hamill, T.G., 2010. Identification of an orally bioavailable, potent, and selective inhibitor of GlyT1. *ACS Med. Chem. Lett.* 1, 350–354. <https://doi.org/10.1021/ml1001085>.
- Daina, A., Zoete, V., 2016. A BOILED-egg to predict gastrointestinal absorption and brain penetration of small molecules. *ChemMedChem* 11, 1117–1121. <https://doi.org/10.1002/cmdc.201600182>.
- Ebenezer, O., Damoyi, N., Jordaan, M.A., Shapi, M., 2022. Unveiling of pyrimidindinones as potential anti-norovirus agents—A pharmacoinformatic-based approach. *Molecules* 27, 380. <https://doi.org/10.3390/molecules27020380>.
- Egan, W.J., Lauri, G., 2002. Prediction of intestinal permeability. *Adv. Drug Delivery Rev.* 54, 273–289. [https://doi.org/10.1016/S0169-409X\(02\)00004-2](https://doi.org/10.1016/S0169-409X(02)00004-2).
- Egan, W.J., Merz, K.M., Baldwin, J.J., 2000. Prediction of drug absorption using multivariate statistics. *J. Med. Chem.* 43, 3867–3877. <https://doi.org/10.1021/jm000292e>.
- El Fadili, M., Er-rajy, M., Imtara, H., Kara, M., Zarougui, S., Altawjry, N., Al kamaly, O., Al Sfouk, A., Elhallaoui, M., 2022a. 3D-QSAR, ADME-Tox In Silico Prediction and Molecular Docking Studies for Modeling the Analgesic Activity against Neuro-pathic Pain of Novel NR2B-Selective NMDA Receptor Antagonists. *Processes* 10, 1462. <https://doi.org/10.3390/pr10081462>.
- El Fadili, M., Er-Rajy, M., Kara, M., Assouguem, A., Belhassan, A., Alotaibi, A., Mrabti, N.N., Fidan, H., Ullah, R., Ercisli, S., Zarougui, S., Elhallaoui, M., 2022b. QSAR, ADMET In Silico Pharmacokinetics, Molecular Docking and Molecular Dynamics Studies of Novel Bicyclo (Aryl Methyl) Benzamides as Potent GlyT1 Inhibitors for the Treatment of Schizophrenia. *Pharmaceuticals* 15, 670. <https://doi.org/10.3390/ph15060670>.
- El Fadili, M., Er-rajy, M., Imtara, H., Noman, O.M., Mothana, R.A., Abdullah, S., Zerougui, S., Elhallaoui, M., 2023. QSAR, ADME-Tox, molecular docking and molecular dynamics simulations of novel selective glycine transporter type 1 inhibitors with memory enhancing properties. *Heliyon* e13706. <https://doi.org/10.1016/j.heliyon.2023.e13706>.
- Er-rajy, M., El Fadili, M., Imtara, H., Saeed, A., Ur Rehman, A., Zarougui, S., Abdullah, S.A., Alahdab, A., Parvez, M.K., Elhallaoui, M., 2023. 3D-QSAR Studies, Molecular Docking, Molecular Dynamic Simulation, and ADMET Proprieties of Novel Pteridinone Derivatives as PLK1 Inhibitors for the Treatment of Prostate Cancer. *Life* 13, 127. <https://doi.org/10.3390/life13010127>.
- Er-rajy, M., El Fadili, M., Hadni, H., Mrabti, N.N., Zarougui, S., Elhallaoui, M., 2022. 2D-QSAR modeling, drug-likeness studies, ADMET prediction, and molecular docking for anti-lung cancer activity of 3-substituted-5-(phenylamino) indolone derivatives. *Struct. Chem.* 33, 973–986. <https://doi.org/10.1007/s11224-022-01913-3>.
- Er-Rajy, M., El Fadili, M., Mrabti, N.N., Zarougui, S., Elhallaoui, M., 2022. QSAR, molecular docking, ADMET properties in silico studies for a series of 7-propanamide benzoxaboroles as potent anti-cancer agents. *Chinese J. Anal. Chem.* 50,. <https://doi.org/10.1016/j.cjac.2022.100163> 100163.
- Er-rajy, M., El Fadili, M., Mujwar, S., Zarougui, S., Elhallaoui, M., 2023a. Design of novel anti-cancer drugs targeting TRKs inhibitors based 3D QSAR, molecular docking and molecular dynamics simulation. *Journal of Biomolecular Structure and Dynamics* 0, 1–14 <https://doi.org/10.1080/07391102.2023.2170471>.
- Er-rajy, M., Fadili, M.E., Mujwar, S., Lenda, F.Z., Zarougui, S., Elhallaoui, M., 2023b. QSAR, molecular docking, and molecular dynamics simulation-based design of novel anti-cancer drugs targeting thioredoxin reductase enzyme. *Struct Chem* <https://doi.org/10.1007/s11224-022-02111-x>.
- Eulenburg, V., Armsen, W., Betz, H., Gomeza, J., 2005. Glycine transporters: essential regulators of neurotransmission. *Trends Biochem. Sci.* 30, 325–333. <https://doi.org/10.1016/j.tibs.2005.04.004>.
- Faisal, S., Badshah, S.L., Kubra, B., Sharaf, M., Emwas, A.-H., Jaremko, M., Abdalla, M., 2022. Identification and inhibition of the druggable allosteric site of SARS-CoV-2 NSP10/NSP16 methyltransferase through computational approaches. *Molecules* 27, 5241. <https://doi.org/10.3390/molecules27165241>.
- Golbraikh, A., Tropsha, A., 2002. Beware of q²! *J. Mol. Graph. Model.* 20, 269–276. [https://doi.org/10.1016/S1093-3263\(01\)00123-1](https://doi.org/10.1016/S1093-3263(01)00123-1).
- Groth, D., Hartmann, S., Klie, S., Selbig, J., 2013. Principal components analysis. *Comput. Toxicol.* 527–547. https://doi.org/10.1007/978-1-62703-059-5_22.
- Guerra Tort, C., Aguiar Pulido, V., Suárez Ulloa, V., Docampo Boedo, F., López Gestal, J.M., Pereira Loureiro, J., 2020. Electronic Health Records Exploitation Using Artificial Intelligence Techniques, in: 3rd XoveTIC Conference. Presented at the XoveTIC Conference, MDPI, p. 60. <https://doi.org/10.3390/proceedings2020054060>.
- Halder, A.K., Jha, T., 2010. Validated predictive QSAR modeling of N-aryl-oxazolindione-5-carboxamides for anti-HIV protease activity. *Bioorg. Med. Chem. Lett.* 20, 6082–6087. <https://doi.org/10.1016/j.bmcl.2010.08.050>.
- Hollingsworth, S.A., Dror, R.O., 2018. Molecular dynamics simulation for all. *Neuron* 99, 1129–1143. <https://doi.org/10.1016/j.neuron.2018.08.011>.
- Hu, X., Zeng, Z., Zhang, J., Wu, D., Li, H., Geng, F., 2023. Molecular dynamics simulation of the interaction of food proteins with small

- molecules. *Food Chem.* 405,. <https://doi.org/10.1016/j.foodchem.2022.134824> 134824.
- Hudson, A.R., Santora, V.J., Petroski, R.E., Almos, T.A., Anderson, G., Barido, R., Basinger, J., Bellows, C.L., Bookser, B.C., Broadbent, N.J., Cabebe, C., Chai, C.-K., Chen, M., Chow, S., Chung, D.M., Heger, L., Danks, A.M., Freestone, G.C., Gitnick, D., Gupta, V., Hoffmaster, C., Kaplan, A.P., Kennedy, M.R., Lee, D., Limberis, J., Ly, K., Mak, C.C., Masatsugu, B., Morse, A.C., Na, J., Neul, D., Nikpur, J., Renick, J., Sebring, K., Sevidal, S., Tabatabaei, A., Wen, J., Xia, S., Yan, Y., Yoder, Z.W., Zook, D., Peters, M., Breitenbucher, J.G., 2020. Azetidine-based selective glycine transporter-1 (GlyT1) inhibitors with memory enhancing properties. *Bioorg. Med. Chem. Lett.* 30,. <https://doi.org/10.1016/j.bmcl.2020.127214> 127214.
- Jia, C.-Y., Li, J.-Y., Hao, G.-F., Yang, G.-F., 2020. A drug-likeness toolbox facilitates ADMET study in drug discovery. *Drug Discov. Today* 25, 248–258. <https://doi.org/10.1016/j.drudis.2019.10.014>.
- Kaminski, G.A., Friesner, R.A., Tirado-Rives, J., Jorgensen, W.L., 2001. Evaluation and reparametrization of the OPLS-AA force field for proteins via comparison with accurate quantum chemical calculations on peptides. *J. Phys. Chem. B* 105, 6474–6487. <https://doi.org/10.1021/jp003919d>.
- Karplus, M., McCammon, J.A., 2002. Molecular dynamics simulations of biomolecules. *Nat. Struct. Biol.* 9, 646–652. <https://doi.org/10.1038/nsb0902-646>.
- Kouranov, A., 2006. The RCSB PDB information portal for structural genomics. *Nucleic Acids Res.* 34, D302–D305. <https://doi.org/10.1093/nar/gkj120>.
- Kravić, N., Savosina, J., Agafonova-Moroz, M., Babain, V., Legin, A., Kirsanov, D., 2022. Nonlinear multivariate regression algorithms for improving precision of multisensor potentiometry in analysis of spent nuclear fuel reprocessing solutions. *Chemosensors* 10, 90. <https://doi.org/10.3390/chemosensors10030090>.
- Łatka, K., Bajda, M., 2022. Analysis of binding determinants for different classes of competitive and noncompetitive inhibitors of glycine transporters. *IJMS* 23, 8050. <https://doi.org/10.3390/ijms23148050>.
- Lipinski, C.A., Lombardo, F., Dominy, B.W., Feeney, P.J., 1997. Experimental and computational approaches to estimate solubility and permeability in drug discovery and development settings. *Adv. Drug Deliv. Rev.* 23, 3–25. [https://doi.org/10.1016/S0169-409X\(96\)00423-1](https://doi.org/10.1016/S0169-409X(96)00423-1).
- Lowe, J.A., Hou, X., Schmidt, C., David Tingley, F., McHardy, S., Kalman, M., DeNinno, S., Sanner, M., Ward, K., Lebel, L., Tunucci, D., Valentine, J., 2009. The discovery of a structurally novel class of inhibitors of the type 1 glycine transporter. *Bioorg. Med. Chem. Lett.* 19, 2974–2976. <https://doi.org/10.1016/j.bmcl.2009.04.035>.
- Maćkiewicz, A., Ratajczak, W., 1993. Principal components analysis (PCA). *Comput. Geosci.* 19, 303–342. [https://doi.org/10.1016/0098-3004\(93\)90090-R](https://doi.org/10.1016/0098-3004(93)90090-R).
- Milne, G.W.A., 2010. Software Review of ChemBioDraw 12.0. *J. Chem. Inf. Model.* 50, 2053–2053. <https://doi.org/10.1021/ci100385n>.
- Mostoufi, N., Constantinides, A., 2023. Linear and nonlinear regression analysis, in: *Applied Numerical Methods for Chemical Engineers*. Elsevier, pp. 403–476. <https://doi.org/10.1016/B978-0-12-822961-3.00008-X>.
- Muegge, I., Heald, S.L., Brittelli, D., 2001. Simple selection criteria for drug-like chemical matter. *J. Med. Chem.* 44, 1841–1846. <https://doi.org/10.1021/jm015507e>.
- Norgan, A.P., Coffman, P.K., Kocher, J.-P.-A., Katzmann, D.J., Sosa, C.P., 2011. Multilevel parallelization of AutoDock 4.2. *J. Cheminform.* 3, 12. <https://doi.org/10.1186/1758-2946-3-12>.
- Ononamadu, C.J., Abdalla, M., Ihegboro, G.O., Li, J., Owolarafe, T. A., John, T.D., Tian, Q., 2021. In silico identification and study of potential anti-mosquito juvenile hormone binding protein (MJHBP) compounds as candidates for dengue virus - Vector insecticides. *Biochem. Biophys. Rep.* 28,. <https://doi.org/10.1016/j.bbrep.2021.101178> 101178.
- Österberg, T., Norinder, U., 2001. Prediction of drug transport processes using simple parameters and PLS statistics The use of ACD/logP and ACD/ChemSketch descriptors. *Eur. J. Pharm. Sci.* 12, 327–337. [https://doi.org/10.1016/S0928-0987\(00\)00189-5](https://doi.org/10.1016/S0928-0987(00)00189-5).
- Ouellet, D., Sutherland, S., Wang, T., Griffini, P., Murthy, V., 2011. First-time-in-human study with GSK1018921, a selective GlyT1 inhibitor: Relationship between exposure and dizziness. *Clin. Pharmacol. Ther.* 90, 597–604. <https://doi.org/10.1038/clpt.2011.154>.
- Pinard, E., Alanine, A., Alberati, D., Bender, M., Borroni, E., Bourdeaux, P., Brom, V., Burner, S., Fischer, H., Hainzl, D., Halm, R., Hauser, N., Jolidon, S., Lengyel, J., Marty, H.-P., Meyer, T., Moreau, J.-L., Mory, R., Narquizian, R., Nettekoven, M., Norcross, R.D., Puellmann, B., Schmid, P., Schmitt, S., Stalder, H., Wermuth, R., Wettstein, J.G., Zimmerli, D., 2010a. Selective GlyT1 inhibitors: Discovery of [4-(3-Fluoro-5-trifluoromethylpyridin-2-yl)piperazin-1-yl][5-methanesulfonyl-2-((S)-2,2,2-trifluoro-1-methylethoxy)phenyl]methanone (RG1678), a promising novel medicine to treat schizophrenia. *J. Med. Chem.* 53, 4603–4614. <https://doi.org/10.1021/jm100210p>.
- Pires, D.E.V., Blundell, T.L., Ascher, D.B., 2015. pkCSM: Predicting small-molecule pharmacokinetic and toxicity properties using graph-based signatures. *J. Med. Chem.* 58, 4066–4072. <https://doi.org/10.1021/acs.jmedchem.5b00104>.
- Pyrhönen, J., Bansal, K.K., Bhadane, R., Wilén, C.-E., Salo-Ahen, O. M.H., Rosenholm, J.M., 2022. Molecular dynamics prediction verified by experimental evaluation of the solubility of different drugs in poly(decylactone) for the fabrication of polymeric nanoemulsions. *Adv. NanoBiomed. Res.* 2, 2100072. <https://doi.org/10.1002/anbr.202100072>.
- Rafalo, M., 2022. Cross validation methods: Analysis based on diagnostics of thyroid cancer metastasis. *ICT Express* 8, 183–188. <https://doi.org/10.1016/j.icte.2021.05.001>.
- Rezende, K.B. de C., Cunha, A.J.L.A. da, Amim Junior, J., Bornaia, R. G., 2019. External validation of the Fetal Medicine Foundation algorithm for the prediction of preeclampsia in a Brazilian population. *Pregnancy Hypertension* 17, 64–68. <https://doi.org/10.1016/j.preghy.2019.05.006>.
- Rosenbrock, H., Desch, M., Wunderlich, G., 2023. Development of the novel GlyT1 inhibitor, iclepertin (BI 425809), for the treatment of cognitive impairment associated with schizophrenia. *Eur. Arch. Psychiatry Clin. Neurosci.* <https://doi.org/10.1007/s00406-023-01576-z>.
- Santora, V.J., Almos, T.A., Barido, R., Basinger, J., Bellows, C.L., Bookser, B.C., Breitenbucher, J.G., Broadbent, N.J., Cabebe, C., Chai, C.-K., Chen, M., Chow, S., Chung, D.M., Crickard, L., Danks, A.M., Freestone, G.C., Gitnick, D., Gupta, V., Hoffmaster, C., Hudson, A.R., Kaplan, A.P., Kennedy, M.R., Lee, D., Limberis, J., Ly, K., Mak, C.C., Masatsugu, B., Morse, A.C., Na, J., Neul, D., Nikpur, J., Peters, M., Petroski, R.E., Renick, J., Sebring, K., Sevidal, S., Tabatabaei, A., Wen, J., Yan, Y., Yoder, Z.W., Zook, D., 2018. Design and synthesis of novel and selective glycine transporter-1 (GlyT1) inhibitors with memory enhancing properties. *J. Med. Chem.* 61, 6018–6033. <https://doi.org/10.1021/acs.jmedchem.8b00372>.
- Serrano, A., Imbernón, B., Pérez-Sánchez, H., Cecilia, J.M., Bueno-Crespo, A., Abellán, J.L., 2020. QN-Docking: An innovative molecular docking methodology based on Q-Networks. *Appl. Soft Comput.* 96,. <https://doi.org/10.1016/j.asoc.2020.106678> 106678.
- SwissADME [WWW Document], n.d. URL <http://www.swissadme.ch/> (accessed 1.7.23).
- Systèmes, D., 2020. Free Download: BIOVIA Discovery Studio Visualizer [WWW Document]. Dassault Systèmes. URL <https://discover.3ds.com/discovery-studio-visualizer-download> (accessed 1.7.23).

- TANWER, S., Shukla, S., 2023. Cefuroxime: A Potential Corrosion Inhibitor for Mild Steel in Sulphuric Acid Medium. *Prog. Color Colorants Coat.* 16. <https://doi.org/10.30509/pccc.2022.166974.1165>.
- Tian, S., Wang, J., Li, Y., Li, D., Xu, L., Hou, T., 2015. The application of in silico drug-likeness predictions in pharmaceutical research. *Adv. Drug Deliv. Rev.* 86, 2–10. <https://doi.org/10.1016/j.addr.2015.01.009>.
- Uyanık, G.K., Güler, N., 2013. A study on multiple linear regression analysis. *Procedia. Soc. Behav. Sci.* 106, 234–240. <https://doi.org/10.1016/j.sbspro.2013.12.027>.
- Veber, D.F., Johnson, S.R., Cheng, H.-Y., Smith, B.R., Ward, K.W., Kopple, K.D., 2002. Molecular properties that influence the oral bioavailability of drug candidates. *J. Med. Chem.* 45, 2615–2623. <https://doi.org/10.1021/jm020017n>.
- Vilar, S., Cozza, G., Moro, S., 2008. Medicinal chemistry and the molecular operating environment (MOE): Application of QSAR and molecular docking to drug discovery. *CTMC* 8, 1555–1572. <https://doi.org/10.2174/156802608786786624>.
- Wang, Y., Zhao, H., Brewer, J.T., Li, H., Lao, Y., Amberg, W., Behl, B., Akritopoulou-Zanze, I., Dietrich, J., Lange, U.E.W., Pohlki, F., Hoft, C., Hornberger, W., Djuric, S.W., Sydor, J., Mezler, M., Relo, A.L., Vasudevan, A., 2018. De Novo design, synthesis, and biological evaluation of 3,4-disubstituted pyrrolidine sulfonamides as potent and selective glycine transporter 1 competitive inhibitors. *J. Med. Chem.* 61, 7486–7502. <https://doi.org/10.1021/acs.jmedchem.8b00295>.
- Wolkenberg, S., Sur, C., 2010. Recent progress in the discovery of non-sarcosine based GlyT1 inhibitors. *CTMC* 10, 170–186. <https://doi.org/10.2174/156802610790410974>.
- Wolkenberg, S.E., Zhao, Z., Wisnoski, D.D., Leister, W.H., O'Brien, J., Lemaire, W., Williams, D.L., Jacobson, M.A., Sur, C., Kinney, G.G., Pettibone, D.J., Tiller, P.R., Smith, S., Gibson, C., Ma, B.K., Polsky-Fisher, S.L., Lindsley, C.W., Hartman, G.D., 2009. Discovery of GlyT1 inhibitors with improved pharmacokinetic properties. *Bioorg. Med. Chem. Lett.* 19, 1492–1495. <https://doi.org/10.1016/j.bmcl.2009.01.015>.
- Zentrum für Bioinformatik: Universität Hamburg - Proteins Plus Server [WWW Document], n.d. URL <https://proteins.plus/> (accessed 1.15.23).